Hydrogen Spillover through Hydride Transfer: The Reaction of ZnO and ZrO_2 with Strong Hydride Donors

Michael Benz,[a] Osman Bunjaku,[a] Michal Nowakowski,[b] Alexander Allgaier,[a] Indro Biswas,[c] Joris van Slageren,[a] Matthias Bauer,[b] and Deven P. Estes*[a]

[a] M. Benz, O. Bunjaku, A. Allgaier, Prof. Dr. J. van Slageren, and Jun.-Prof. Dr. D. P. Estes
Department of Chemistry
University of Stuttgart
Pfaffenwaldring 55, 70569 Stuttgart, Germany.
E-mail: deven.estes@itc.uni-stuttgart.de

[b] Dr. M. Nowakowski, Prof. Dr. M. Bauer
Department of Chemistry
University of Paderborn
Warburger Straße 100, 33098 Paderborn, Germany.

[c] Dr. Indro Biswas
Department of Electrochemical Energy Technology, Institute of Engineering Thermodynamics,
German Aerospace Centre (DLR)
70569 Stuttgart, Germany

Supporting Information

General Experimental

All experiments were performed under nitrogen or argon using standard Schlenk and glovebox techniques. $HV(CO)_4dppe$[1] and $CpCr(CO)_3H$[2] were synthesized by standard procedures. ZnO (hexagonal, $P6_3mc$, 9.77 m^2g^{-1}) and ZrO_2 (monoclinic, $P2_1/c$, 70.8 m^2g^{-1}) were obtained from commercial sources and used as received. Acetonitrile, toluene, and pentane were purified using an M-Braun Solvent Purification System by sparging with Ar and passage through a column of activated alumina. Deuterated benzene was purified by degassing via three freeze-pump-thaw cycles and stored over activated molecular sieves (4Å) to dry.

BET surface areas were measured using an autosorb iQ physisorption instrument with N_2 at 77K. Samples were degassed for 8h at 300 °C prior to measurement. IR spectra were measured on a Nicolet 6700 IR spectrometer in transmission mode on samples as KBr pellets. IR spectra of air sensitive samples were measured under inert atmosphere (Ar) using a homemade pellet holder inside a glass cell with CaF_2 windows. Liquid-state NMR spectra were measured on a 400 MHz Bruker AVIII spectrometer in J-young tubes in C_6D_6. Solid-state NMR spectra were measured in 4mm zirconia rotors with a MAS frequency of 11 kHz on a 400 MHz Bruker AVIII spectrometer. EPR spectra were measured of solid powdered samples that had been washed and dried on a cw X-band EMX spectrometer at liquid nitrogen temperature in 4 mm quartz tubes outfitted with a glass cap that can be sealed under argon or evacuated to 10^{-5} mbar. EPR spectral simulations were carried out using the EasySpin toolbox for MATLAB.[3] Photoelectron and Auger electron spectra were recorded on a photoelectron spectrometer with a hemispherical electron analyser and a base pressure of $2x10^{-10}$ mbar (ThermoScientific / FEI ESCALAB Xi^+), using monochromated Al Kα radiation with an energy of 1486.7 eV.

EXAFS measurements

EXAFS data were collected at the P65 beamline, Petra III, Hamburg (DESY). Energy selection was conducted using a Si(111) double crystal monochromator, providing approx.1.1 eV resolution at 9 keV. The beam spot size was 0.5 x 1 mm^2, resulting in flux on sample 10^{12} ph/s. Beam focusing and higher harmonic rejections was done using Rh-coated mirrors. The

measurement was conducted in fluorescence mode using a standard PIPS detector. Data acquisition was performed in the continuous scanning mode, and spectra were rebinned afterwards. Energy calibration was conducted at the first inflection point of the pure Cu XANES spectrum (8977.3 eV). To avoid radiation damage, each EXAFS spectrum was collected at a different sample position.

Data reduction: normalization and background removal were conducted with the Athena software. EXAFS fitting was performed with the Artemis package using the Multiple Scattering approach in R-space. The fitting procedures were done in an R-range of 1.0-4.0 Å and a k-range of 2.0 – 12.5 $Å^{-1}$ on k^2 – weighted spectra. The linear combination fitting analysis was performed in Athena software with boundary on weights limited to [0,1]. Due to the good quality of data, the XANES region fits were performed on I^{st} derivative spectra in the range of -20 – 50 eV around the absorption edge's first inflection point.

Theoretical calculations

Ab-initio calculations were conducted with the FEFF 9.6 software. Computations were done within the Full Multiple Scattering theory using muffin-tin atomic potentials optimized in the Self-Consistent Field (SCF) approach. For H atoms, the muffin-tin overlap factor (FOLP) was reduced to 0.8. The FMS and SCF radii were set to 7.0 Å. For both calculations, the partially-nonlocal exchange–correlation potential and final state rule core-hole screening were applied.[4] From the total DOS functions, occupied and unoccupied contributions were obtained by multiplication of each lDOS function by the arctangent step function broadened by the Cu 1s core-hole lifetime at the Fermi level given by FMS calculations. The experimental resolution of 1.1 eV was included in the calculations. The model structure was taken from the CCDC Database under 1864974.cif entry (CSD identifier: QIKDOG).

TEM EDX

TEM EDX images were recorded using a ThermoFisher Spectra 300 at the SRF AMICA (Stuttgart Research Focus Advanced Materials Innovation and Characterization) at the University of Stuttgart. The system was operated in STEM mode, at an acceleration voltage of 300 kV, a beam convergence angle of 10 or 22 mrad, a camera length of 115 or 145 mm, and a beam current of 50-150 pA. A HAADF detector and a SuperX-G2 EDX detector were used to record the data. The samples were allowed to slowly oxidize over night via diffusion of air through a needle and before dispersion of the samples on Ni grids for measurement.

*Synthesis of **5**-d_6 deuterated Stryker's reagent [$(Ph_3P)CuD]_6$*

The compound was synthesized by the method of Lee and Yun[5]:

$$6Cu(acetate)_2 + 6P(C_6H_5)_3 + 3(C_6H_5)_2SiD_2 \rightarrow [DCu\{P(C_6H_5)_3\}]_6 + 3(C_6H_5)_2Si(acetate)_2$$

In a Schlenk flask anhydrous $Cu(acetate)_2$ (0.522 g, 2.86 mmol) and $P(C_6H_5)_3$ (1.50 g, 5.72 mmol) were dissolved in anhydrous toluene (6 mL). $(C_6H_5)_2SiD_2$ (Aldrich, 97% D) (0.60 g, 3.22 mmol) was added to the reaction mixture and stirred for 3 h. After the color change to a red solution, the mixture was reduced to ½ its volume and allowed to settle under vacuum. Anhydrous acetonitrile (15 mL) was added carefully under argon and crystallisation allowed to occur overnight. The red/orange crystals were filtered using a cannula fitted with a filter apparatus and washed with anhydrous acetonitrile (5x15 mL). The product was dried under vacuum, analysed by ^{1}H NMR and stored under argon for further use (0.71 g, 2.17 mmol, 75,7% yield).

^{1}H NMR (400 MHz, C_6D_6, δ): 7.67 (t, 36H, J = 8.0 Hz), 6.95 (t, 18H, J = 7.3 Hz), 6.74 (t, 36H, J = 7.5 Hz).

*Procedure for reaction of **3-5** with ZnO and ZrO_2*

ZrO_2 and ZnO were dehydroxylated at 500 °C and high vacuum (10^{-5} mbar) for 16 h prior to use. ZrO_2 (0.5 g, 4.06 mmol) or ZnO (0.33 g, 4.06 mmol) was filled into a Schlenk flask and 12.5 mL of a 0.1 M metal hydride solution was added. Therefore 1.25 mL of a 1 M solution of **3** (Aldrich) was diluted with anhydrous THF (Aldrich) to a total volume of 12.5 mL, **4** (Aldrich) (0.322 g, 1.25 mmol) was dissolved in 12.5 mL anhydrous THF and **5** (Aldrich) (0.409 g, 1.25 mmol) was dissolved in 12.5 mL anhydrous toluene. For **5**-d_6 a smaller scale was prepared with ZrO_2 (0.4 g, 3.25 mmol) or ZnO (0.26 g, 3.25 mmol) and a solution of **5**-d_6 (0.328 g, 1.00 mmol) in 10 mL anhydrous toluene. The mixture was stirred overnight at room temperature. After filtration using a cannula fitted with a filter apparatus the solid was washed with the respective anhydrous solvent (3x10 mL) and dried under high vacuum. The product was characterized using ^{1}H MAS NMR, IR, EPR and EXAFS. The number of OH groups on the surfaces was measured by treatment of the surface with excess benzylmagnesium bromide. The toluene produced by deprotonation of the OH groups was quantified by ^{1}H NMR versus ferrocene as internal standard with a 30s delay time between pulses to ensure quantitative integrals.

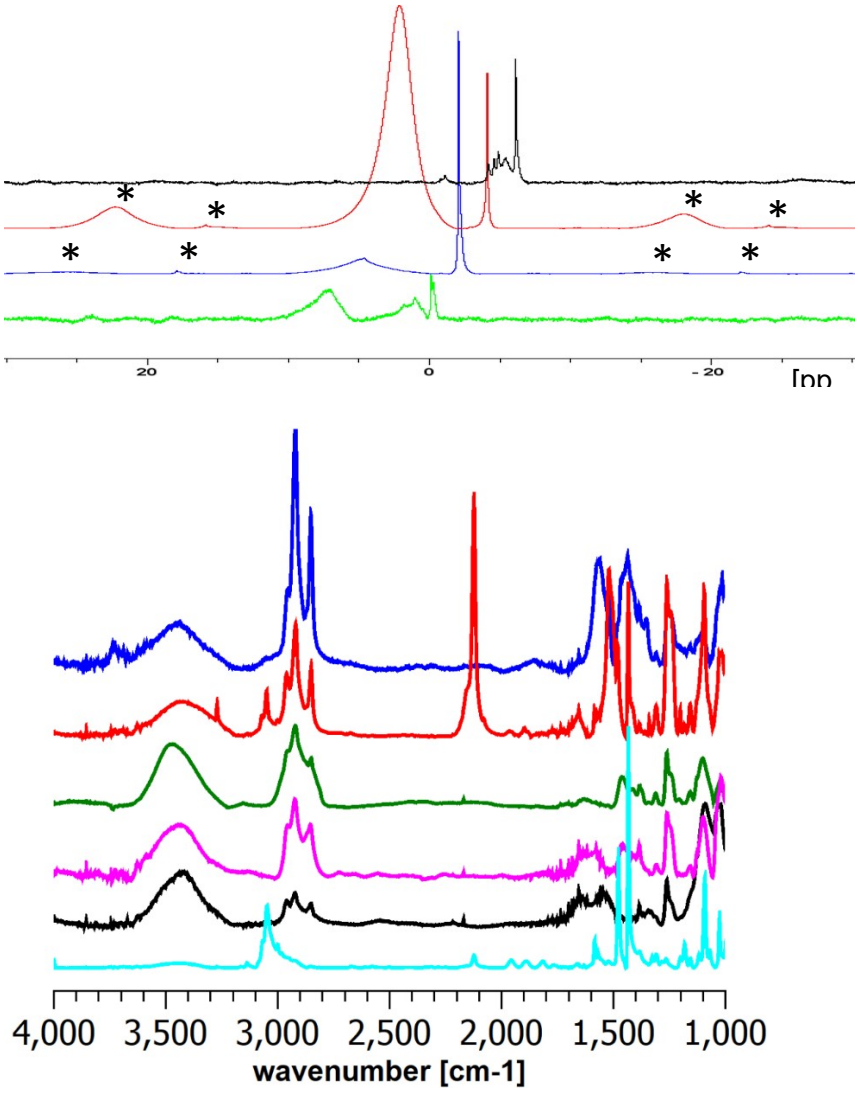

Figure S1. (top) ^{1}H MAS NMR of ZnO after reaction with **3** (black), **4** (red), **5** (blue), and **5**-d_6 (green). (bottom) IR spectra of ZnO (black), **5** (light blue), **3**-ZnO (magenta), **4**-ZnO (green), **5**-ZnO (red), and **5**-d_6-ZnO (blue).

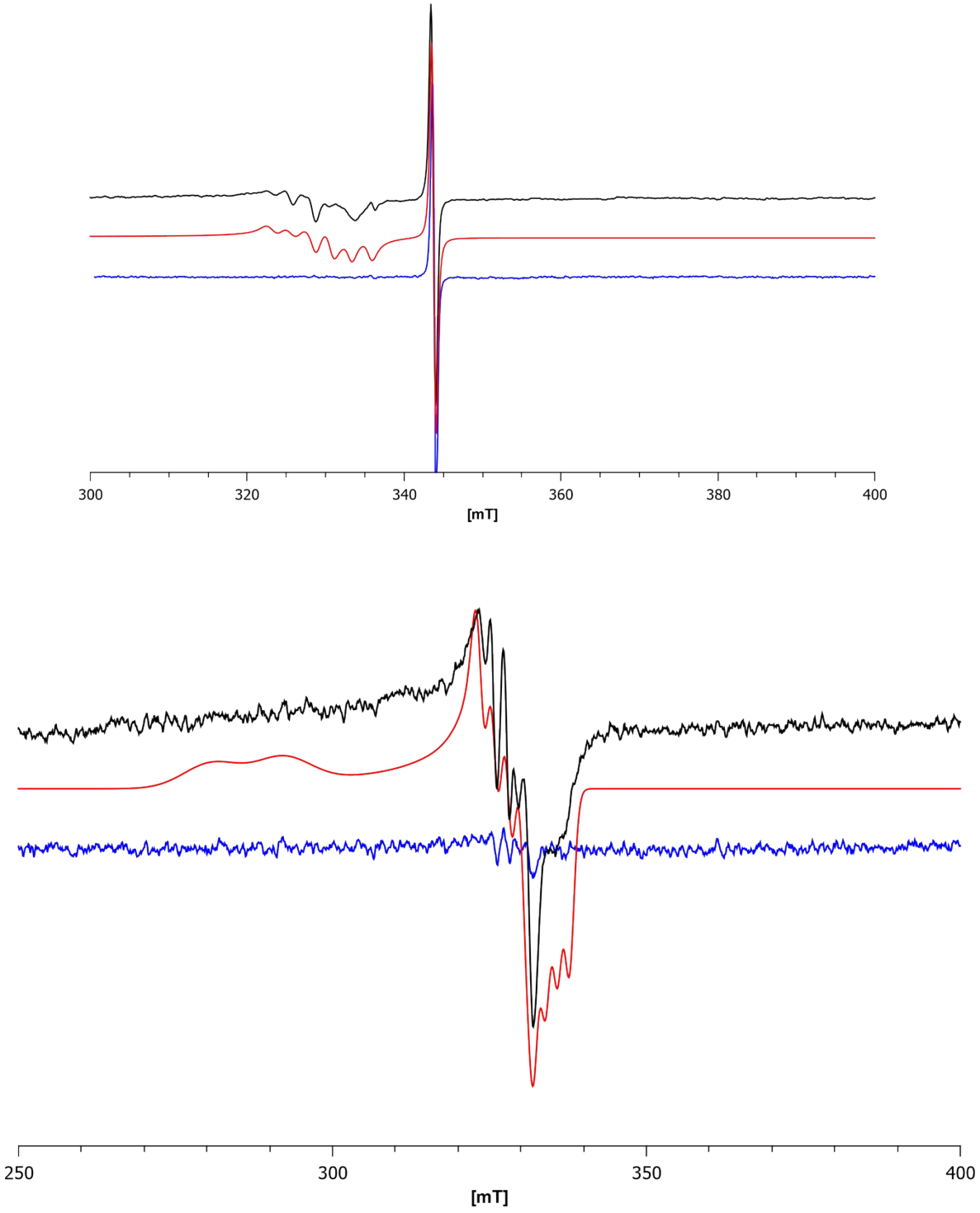

Figure S2. (top) X-Band cwEPR spectra of ZnO reacted with **5** (black; power: 10 mW, modulation amplitude: 8 G) with simulated spectrum (red) and **5**-d_6 (blue; power: 1 mW, modulation amplitude: 8 G) (77 K, evacuated tube). (bottom) X-Band cwEPR spectra of **5** and **5**-d_6 with simulation of the Cu(II) impurity in red (offset between each spectrum).

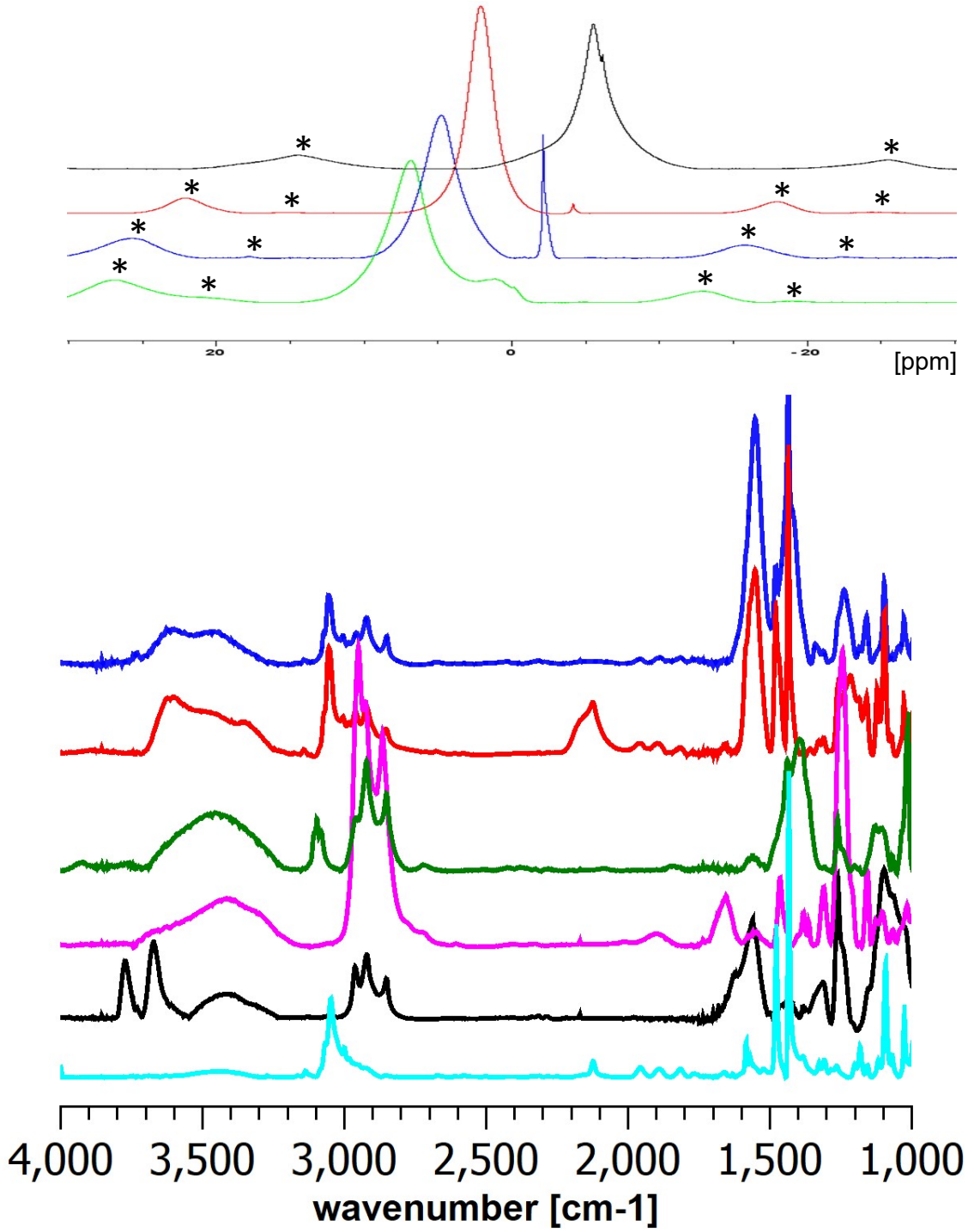

Figure S3. (top) ^{1}H MAS NMR of ZrO_2 after reaction with **3** (black), **4** (red), **5** (blue), and **5**-d_6 (green). (bottom) IR spectra of **5** (light blue), ZrO_2 (black), **3**-ZrO_2 (magenta), **4**-ZrO_2 (green), **5**-ZrO_2 (red), and **5**-d_6-ZrO_2 (blue).

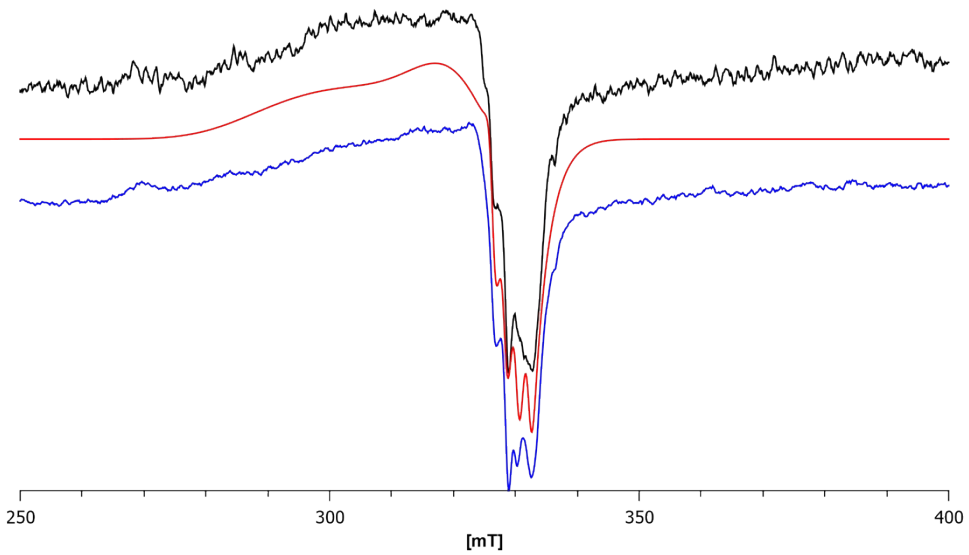

Figure S4. X-Band cwEPR spectra of ZrO_2 reacted with **5** (black; power: 10 mW, modulation amplitude: 8 G) with simulated spectrum (red) and **5**-d_6 (blue; power: 10 mW, modulation amplitude: 8 G) (77 K, evacuated tube).

Table S1. Simulation parameters for X-Band cwEPR measurements of ZnO and ZrO_2 after reaction with **3** – **5**.

Sample	Zn	Zr		Cu			A(Cu) [MHz]			
	g	g_1	g_2	g_1	g_2	g_3	A_1	A_2	A_3	A_4
ZrO_2-**3**	-	1.97	1.91	-	-	-	-	-	-	-
ZrO_2-**4**	-	-	-	-	-	-	-	-	-	-
ZrO_2-**5**	-	-	-	2.27	2.08	2.04	67.3	348.6	44.6	54.6
ZrO_2-**5**-d_6	-	-	-	2.30	2.08	2.04	69.0	327.6	47.4	55.3
ZnO-**3**	1.96	-	-	-	-	-	-	-	-	-
ZnO-**4**	1.96	-	-	-	-	-	-	-	-	-
ZnO-**5**	1.96	-	-	2.30	2.06	2.03	68.0	300.0	20.0	65.0
ZnO-**5**-d_6	1.96	-	-	-	-	-	-	-	-	-
5	-	-	-	2.35	2.06	2.01	27.2	370.9	62.4	52.8
5-d_6	-	-	-	2.39	2.06	2.01	24.1	421.5	74.5	67.0

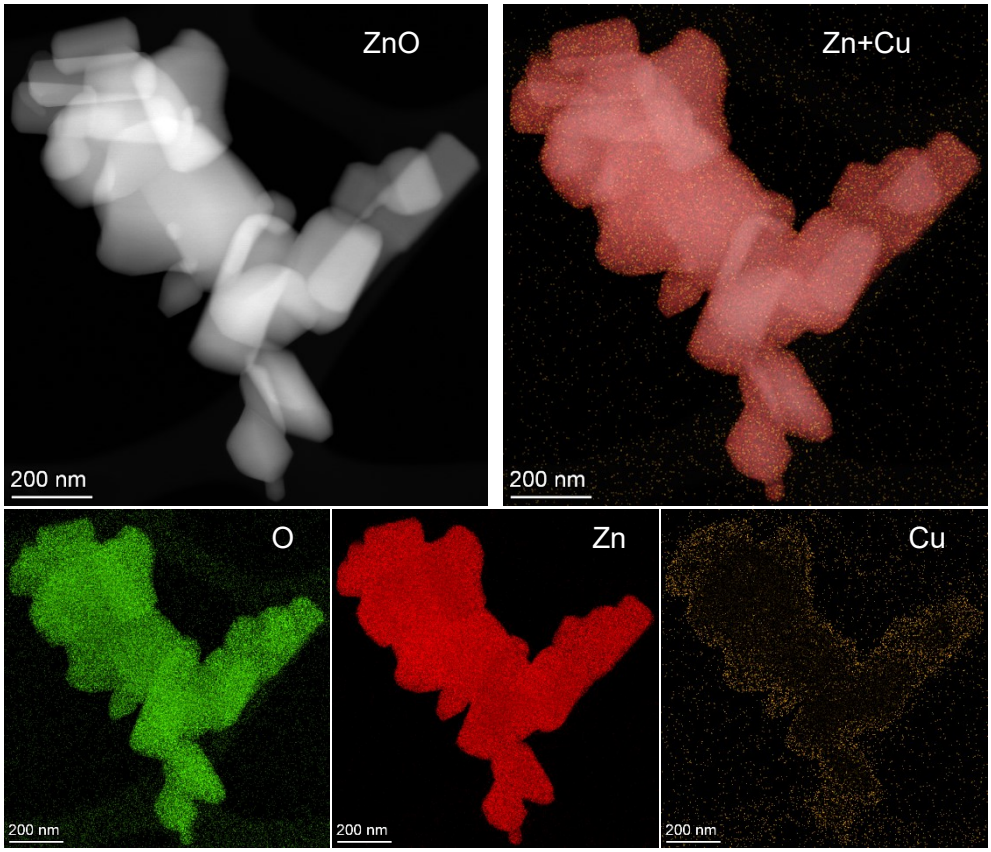

Figure S5. ZnO TEM HAADF image and EDX images for oxygen (green), zinc (red), and copper (yellow).

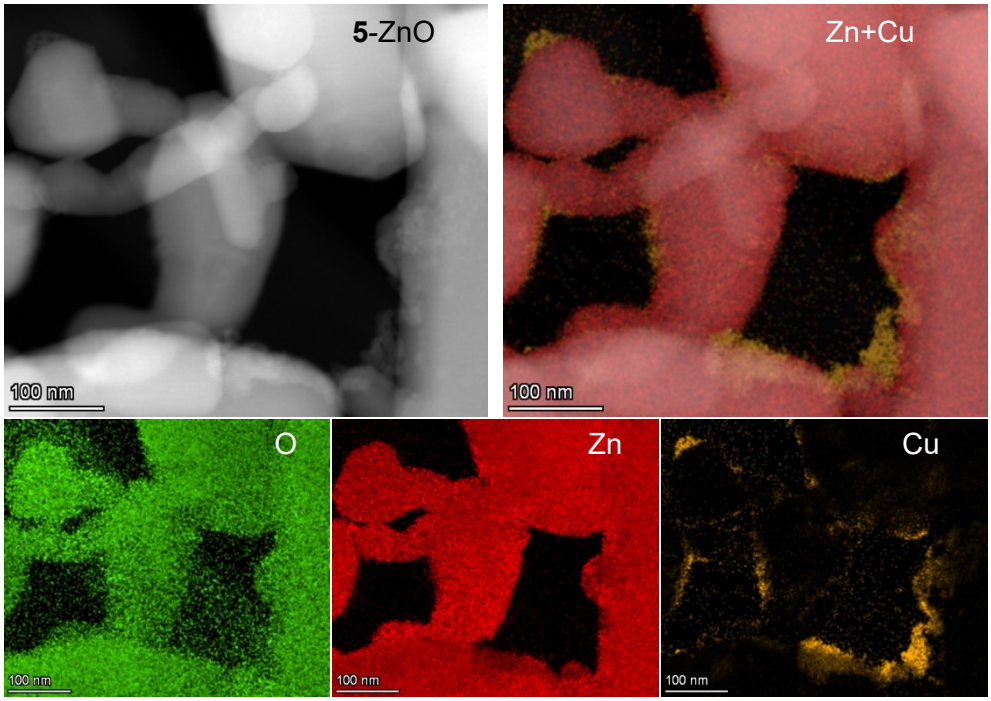

Figure S6. 5-ZnO TEM HAADF image and EDX images for oxygen (green), zinc (red), and copper (yellow).

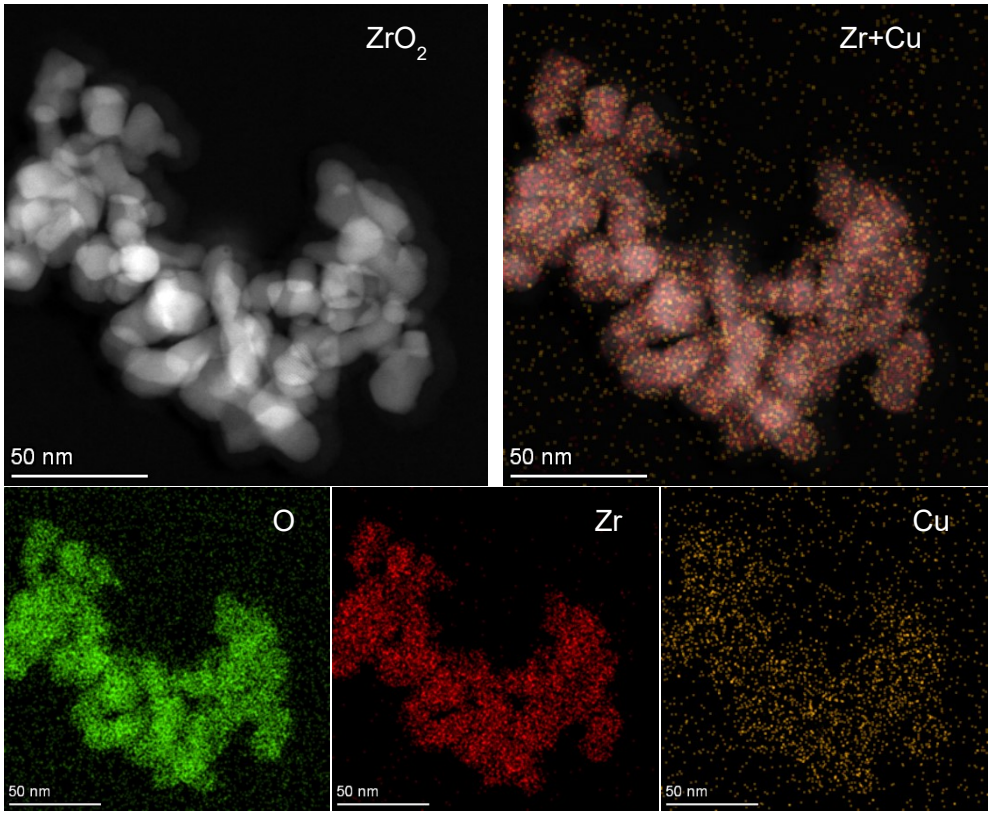

Figure S7. ZrO_2 TEM HAADF image and EDX images for oxygen (green), zirconium (red), and copper (yellow).

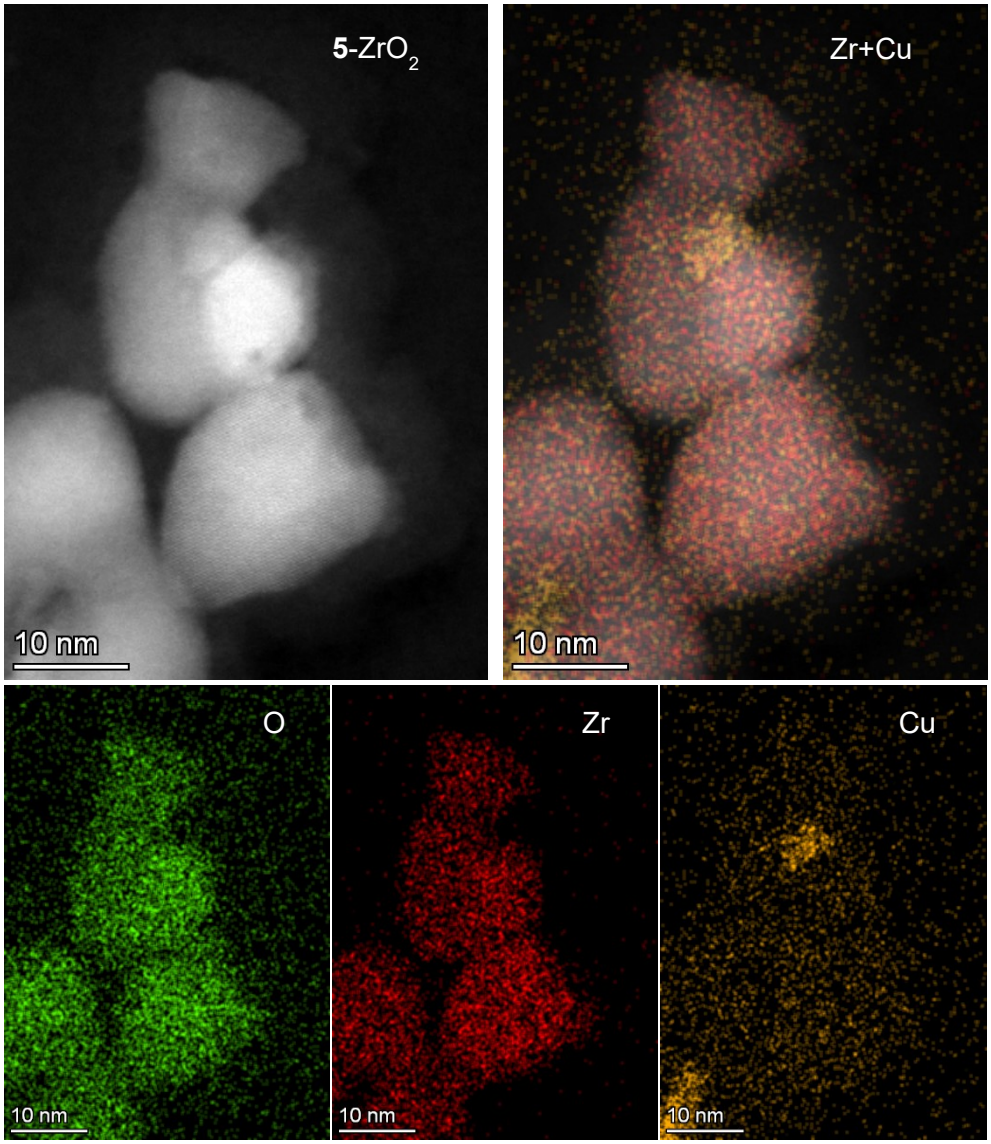

Figure S8. **5**-ZrO_2 TEM HAADF image and EDX images for oxygen (green), zirconium (red), and copper (yellow).

Table S2. TEM EDX quantification of ZnO, **5**-ZnO, ZrO_2, and **5**-ZrO_2 particles.

Element	O at.%	Cu at.%	Zr at.%	Zn at.%
ZrO_2	71.2	(0.46)	28.4	-
5-ZrO_2	70.8	2.78	26.5	-
ZnO	52.2	(0.36)	-	47.5
5-ZnO	43.4	1.62	-	55.0

Extra information about the analysis of the XANES and EXAFS spectra

Figure 5 shows the electronic contributions to the XANES spectrum of **5**. As expected, although H was included in the calculations, its contribution to the XAS spectra is marginal. The structure at 8979 eV has a pre-edge character where unoccupied p-states of Cu and P ligands are hybridized. On the other hand, the white line feature at 8992 eV closely matches the density of states of the unoccupied p orbitals. While we cannot precisely determine the structure of **5**-ZnO and **5**-ZrO_2, we can hypothesize that the support leads to additional relaxation of the Cu 4p and ligand 2p orbitals by admixing more vacant p-type density, along with 3d electron-retraction effect. Such an influence of the solid support on XAS spectra is well-documented. This is an additional factor that could lead to the change in the XANES spectra. Linear combination fitting of the XANES spectrum of **5**-ZnO shows that the amount of Cu(II) is below the detection limit (figure S17). In **5**-ZnO, the 3d-retraction is more evident, thus leading to more prominent hybridization with unoccupied 3d states of Cu. This effect can be compensated by the presence of the H atom's electron density. In **5**-ZrO_2 the donation of unoccupied p-type density is stronger, which increases the white line intensity, but also shifts the energy of the unoccupied p-states to a slightly higher value, leading to lower pre-peak intensity. The final energy position of the absorption edge is not changed, due to the electron density from H atoms.

We also performed linear combination fitting of the XANES spectra to check for the presence of Cu/CuO (observed by TEM). The presence of Cu/CuO domains would severely affect the XAS data. However, in direct comparison in Fig. 5, neither sample resembles Cu(0). Moreover, the linear combination fitting performed using Cu(0), Cu(0), and **5** on **5**-ZnO and **5**-ZrO_2 indicates no Cu(0) or CuO fractions in significant amounts (Fig. S17). In **5**-ZrO_2, a small amount is present in the fit; however, due to the large error bar, it can also be attributed to the shared feature of both **5**-ZrO_2 and CuO XAS spectra, namely the more intense white line. Assuming, for the moment, the contribution is real, such an amount would provide a clear signature in the XAS data and improve the EXAFS fit quality when included, which is not the case here. In fact, the introduction of I^{st} coordination shell Cu-O scatter from CuO significantly deteriorates EXAFS fits of **5**-ZnO and **5**-ZrO_2 beyond recovery. On the other hand, EXAFS indeed shows the progressing decomposition of Stryker's reagent upon contact with the supports Thus, the domains observed in TEM results could be from the next step of the reaction (or potentially even from beam damage during TEM measurements).

To model the EXAFS spectra, it was necessary to include the hydrogen atoms, despite the very low X-ray scattering factor of H. The ability to reproduce the EXAFS signal when H is excluded from the analysis is worse and yields unrealistic results (without H atoms in the fit of complex **5**, EXAFS predicts a coordination number for P of ca. 3, which is much higher than the true value of 1). Hydrogen is visible in the 1^{st} coordination shell peak at. 1.5 Å in Figure 5a (bottom), and can be fitted with the parameters given in Table S2, although the presented differences are not enormous. There is also a difference when the number of H atoms in the fit is fixed according to the initial model or refined. In the latter, the number of H atoms is significantly overestimated, while Debye-Waller factors (σ) are very low (see Tables S2-S4). This can be explained by strong correlations between N and σ in the EXAFS equation, preventing fitting without more assumptions on the model. The same problem was observed for the EXAFS fitting for **5**-ZnO and **5**-ZrO_2. Thus, we believe that the inclusion of H atoms affects the fit quality in the particular case of 1^{st} shell hydrides. However, the number of H atoms obtained has to be interpreted with care, and must be controlled by assumptions on σ or N values. During modelling of 5-ZnO, we compared the model with hydride atoms included, to both the model with a fixed theoretical number of hydrides, and a model with a Cu-O bond. For the

model with a refined number of H atoms, EXAFS analysis indicates 6 H atoms at 1.698(23) Å, one Cu-P scatter at 2.201(24) Å, and two Cu-Cu scatters at 2.512(27) Å. For the model containing a fixed number of H atoms (Debye-Waller factors constrained during the fit), the result was very similar: 4 H atoms at 1.652(19) Å, one Cu-P scatter at 2.123(7) Å, and two Cu-Cu scatters at 2.779(25) Å. In both cases Debye-Waller factors for 2nd and further shells were high, indicating possible problems with both models, as no extra disorder was anticipated. Note that both models required significant anharmonic interactions to be included for convergence. However, the inclusion of the Cu-O bond in the model alleviated these problems and resulted in a better fit with more satisfactory parameters. the same was true of 5-ZrO_2, the data for which was also more satisfactorily modelled by using a Cu-O bond.

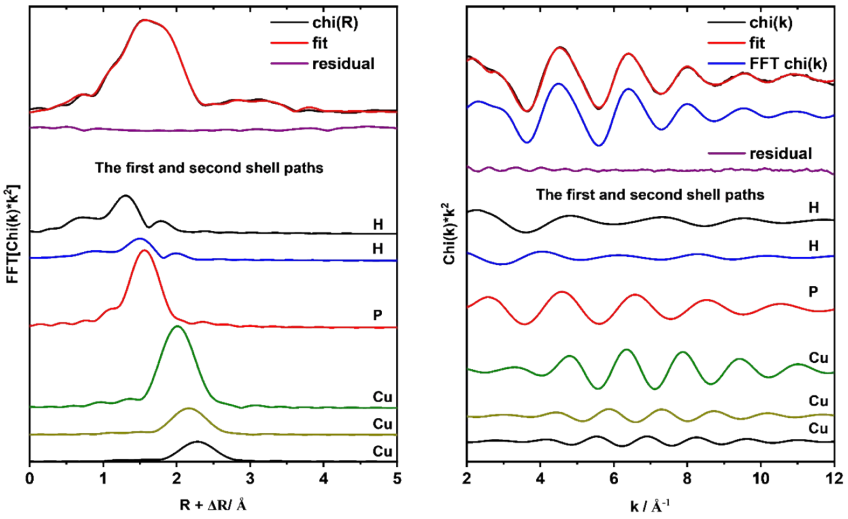

Figure S9. Left: Fourier-transformed EXAFS spectrum of **5** compared to the fitted model, residuals and 1st and 2nd coordination shell scattering paths. Right: k-space EXAFS of **5** compared to the fitted model, Fourier-filtered model, residual function and 1st and 2nd coordination shell scattering paths. The model was fitted without any constrains.

Table S3. Optimized EXAFS parameters for **5** fitted without constraints.

Path	N[a]	σ^2 / Å^2 [b]	R_{eff} / Å [c]	R + ΔR / Å [d]	C_3 / Å^3 [e]
Cu-H	3.4(2)	0.0023(12)	1.735	1.652(24)	0
Cu-H	2.8(2)	0.0023(12)	1.995	1.869(37)	0
Cu-P	1.1(1)	0.0060(20)	2.331	2.204(26)	0.0017(6)
Cu-Cu	2.2(1)	0.0098(12)	2.517	2.517(31)	0.0012(5)
Cu-Cu	0.9(1)	0.0106(11)	2.729	2.675(50)	0.0012(5)
Cu-Cu	0.8(1)	0.0108(11)	2.785	2.799(49)	0.0012(5)
Cu-C	2.5(7)	0.0108(28)	3.585	3.404(109)	0.0025(18)
Cu-P-C	5.4(3.5)	0.0114(34)	3.899	3.840(163)	0.0042(24)
Cu-C	2.8(5)	0.0129(31)	3.972	3.901(57)	0.0025(18)
Cu-C	2.3(5)	0.0113(29)	3.728	4.021(29)	0.0025(18)
Cu-Cu	1.0(3)	0.0113(29)	3.761	4.054(29)	0.0012(5)

[a] – path degeneration / coordination number (for single scattering); [b] – Debye-Waller factor; [c] – distance in structural model used for EXAFS analysis; [d] – fitted distance; [e] – third cumulant (anharmonicity).

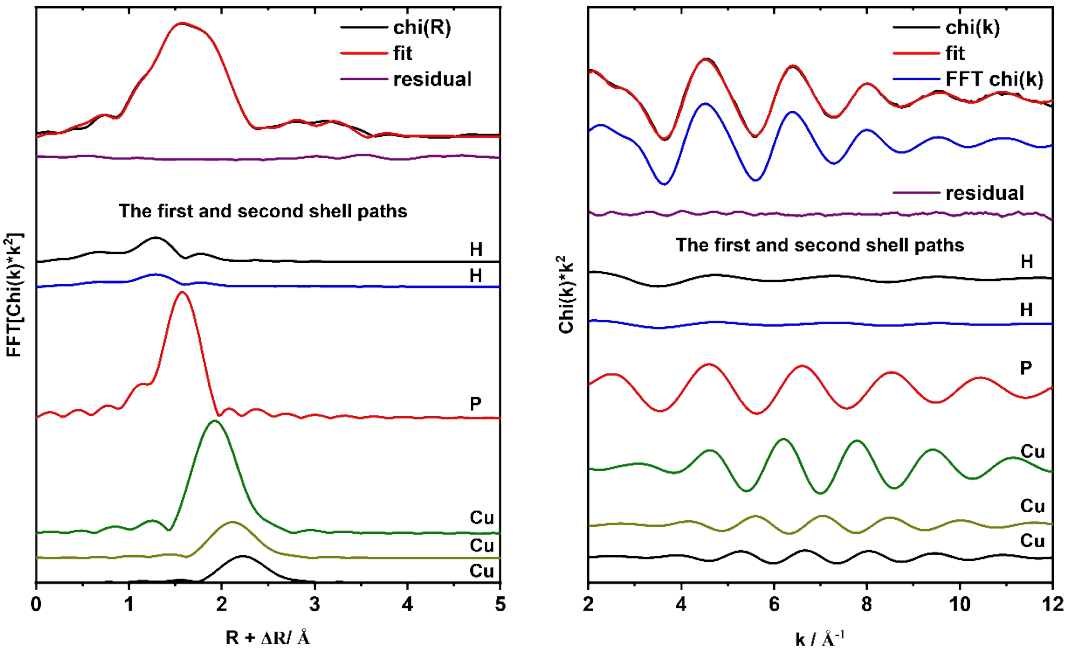

Figure S10. Left: Fourier-transformed EXAFS spectrum of **5** compared to the fitted model, residuals and 1st and 2nd coordination shell scattering paths. Right: k-space EXAFS of **5** compared to the fitted model, Fourier-filtered model, residual function and 1st and 2nd coordination shell scattering paths. The model was fitted with constraints on Debye-Waller factors of Cu-H scatters.

Table S4. Optimized EXAFS parameters for **5** fitted with constrains on Debye-Waller factors of Cu-H scatters.

Path	N[a]	σ^2 / Å^2 [b]	R_{eff} / Å [c]	R + ΔR / Å [d]	C_3 / Å^3 [e]
Cu-H	2.0 (fixed)	0.0031 (fixed)	1.735	1.647(43)	-
Cu-H	1.0 (fixed)	0.0030 (fixed)	1.995	1.644(81)	-
Cu-P	1.1(1)	0.0030(17)	2.331	2.154(19)	0.0010(3)
Cu-Cu	2.2(1)	0.0084(11)	2.517	2.566(52)	0.0022(8)
Cu-Cu	0.9(1)	0.0091(12)	2.729	2.767(82)	0.0022(8)
Cu-Cu	0.8(1)	0.0093(12)	2.785	2.884(63)	0.0022(8)
Cu-P-C	5.4(1.1)	0.0088(33)	3.899	3.668(86)	0.0043(25)
Cu-C	2.5(7)	0.0116(32)	3.585	3.776(40)	0.0033(22)
Cu-C	2.8(1.1)	0.0128(35)	3.972	3.919(71)	0.0033(22)
Cu-C	2.3(1.2)	0.0120(33)	3.728	4.009(33)	0.0033(22)
Cu-Cu	1.0(3)	0.0120(33)	3.761	4.043(33)	0.0022(8)

[a] – path degeneration / coordination number (for single scattering); [b] – Debye-Waller factor; [c] – distance in structural model used for EXAFS analysis; [d] – fitted distance; [e] – third cumulant (anharmonicity).

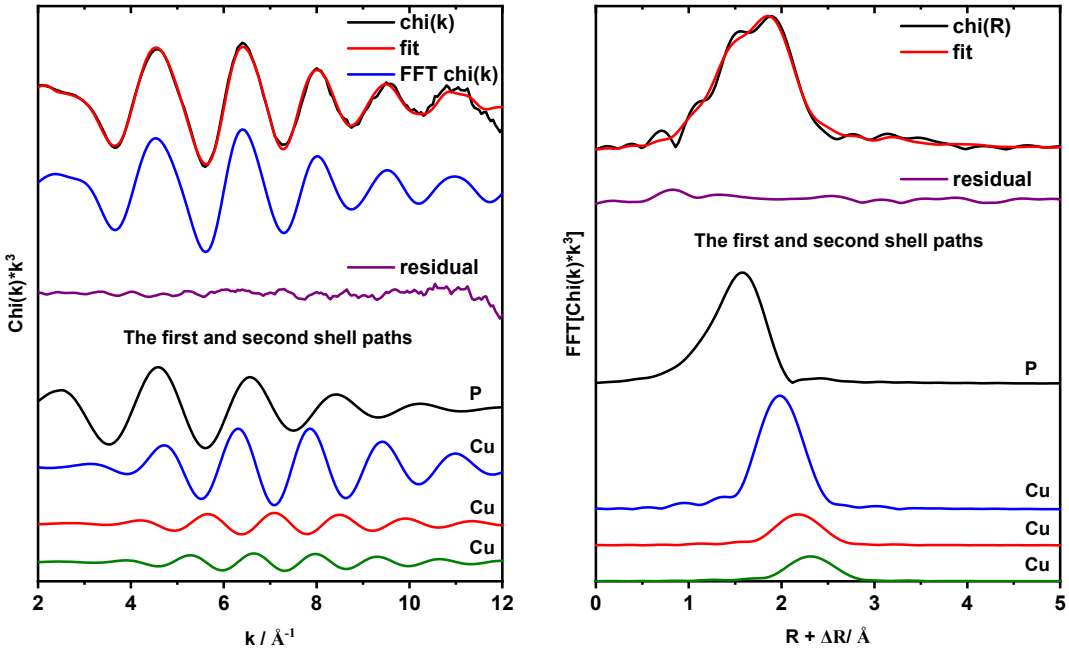

Figure S11. Left: Fourier-transformed EXAFS spectrum of **5** compared to the fitted model, residuals and 1st and 2nd coordination shell scattering paths. Right: k-space EXAFS of **5** compared to the fitted model, Fourier-filtered model, residual function and 1st and 2nd coordination shell scattering paths. The model was fitted without H atoms involved.

Table S5. Optimized EXAFS parameters for **5** fitted without H atoms involved.

Path	N[a]	σ^2 / Å^2 [b]	R_{eff} / Å [c]	R + ΔR / Å [d]	C_3 / Å^3 [e]
Cu-P	2.8(1)	0.0163(4)	2.331	2.139(5)	0.00028(31)
Cu-Cu	2.1(1)	0.0117(7)	2.517	2.486(20)	0.00095(36)
Cu-Cu	0.8(2)	0.0127(7)	2.729	2.698(42)	0.00095(36)
Cu-Cu	0.8(2)	0.0129(7)	2.785	2.838(33)	0.00095(36)
Cu-P-C	5.8(7)	0.0017(48)	3.899	3.636(40)	-0.00916(383)
Cu-C	4.3(2)	0.0079(51)	3.972	3.683(42)	-0.00944(352)

[a] – path degeneration / coordination number (for single scattering); [b] – Debye-Waller factor; [c] – distance in structural model used for EXAFS analysis; [d] – fitted distance; [e] – third cumulant (anharmonicity).

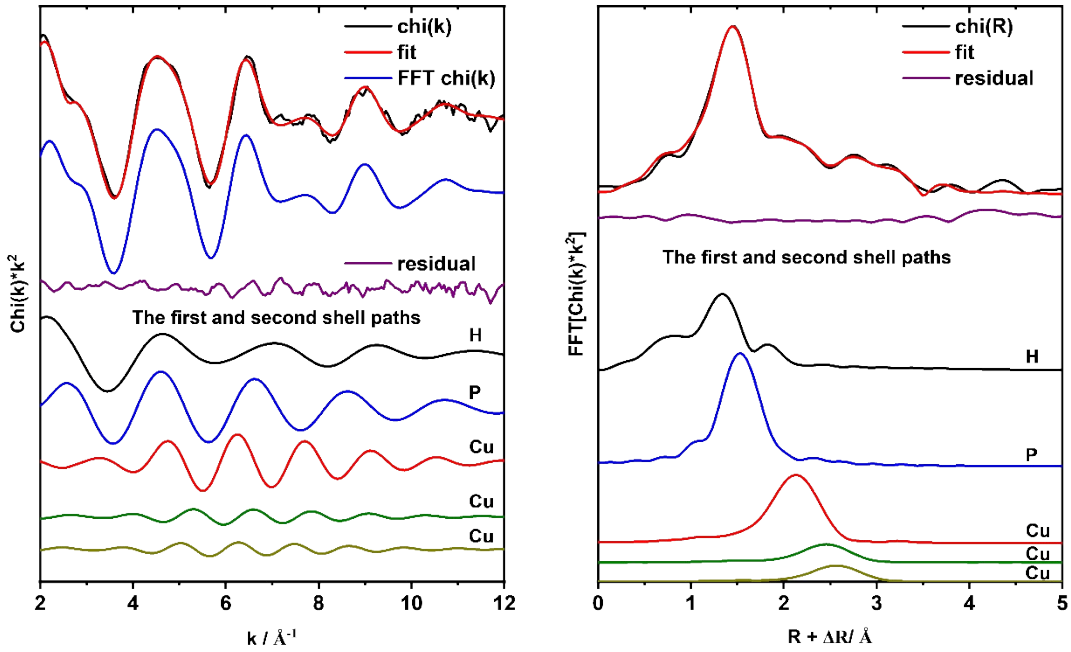

Figure S12. Left: Fourier-transformed EXAFS spectrum of **5**-ZnO compared to the fitted model, residuals and 1st and 2nd coordination shell scattering paths. Right: k-space EXAFS of **5**-ZnO compared to the fitted model, Fourier-filtered model, residual function and 1st and 2nd coordination shell scattering paths. The model was fitted without constrains involved.

Table S6. Optimized EXAFS parameters for **5**-ZnO fitted without constraints.

Path	N[a]	σ^2 / Å^2 [b]	R_{eff} / Å [c]	R + ΔR / Å [d]	C_3 / Å^3 [e]
Cu-H	6.1(5)	0.0048(31)	1.735	1.698(23)	0
Cu-P	1.1(1)	0.0065(15)	2.331	2.201(24)	0.0018(5)
Cu-Cu	2.1(2)	0.0139(12)	2.517	2.512(27)	0.0011(3)
Cu-Cu	0.9(2)	0.0150(13)	2.729	2.864(57)	0.0011(3)
Cu-P-C	7.0(1.6)	0.0114(30)	3.899	2.938(114)	0.0047(26)
Cu-Cu	0.9(3)	0.0154(14)	2.785	2.984(74)	0.0011(3)
Cu-C	2.7(6)	0.0153(95)	3.972	3.272(87)	0.0013(8)
Cu-C	5.1(4)	0.0097(31)	3.585	3.926(26)	0.0013(8)

[a] – path degeneration / coordination number (for single scattering); [b] – Debye-Waller factor; [c] – distance in structural model used for EXAFS analysis; [d] – fitted distance; [e] – third cumulant (anharmonicity).

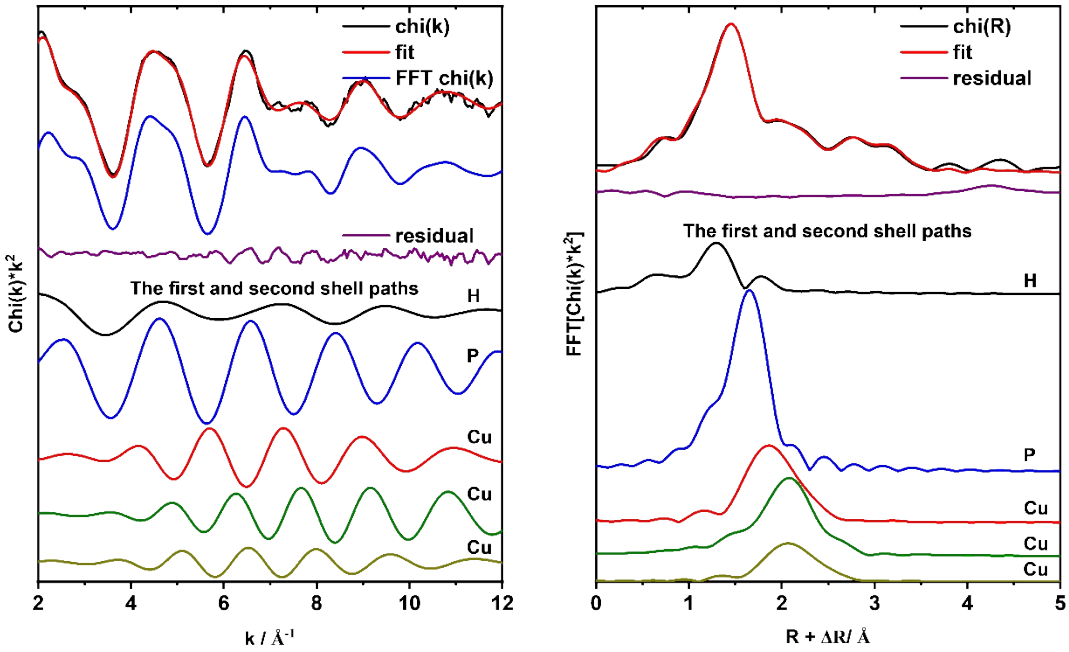

Figure S13. Left: Fourier-transformed EXAFS spectrum of **5**-ZnO compared to the fitted model, residuals and 1st and 2nd coordination shell scattering paths. Right: k-space EXAFS of **5**-ZnO compared to the fitted model, Fourier-filtered model, residual function and 1st and 2nd coordination shell scattering paths. The model was fitted with constraints on Debye-Waller factors of Cu-H scatters.

Table S7. Optimized EXAFS parameters for **5**-ZnO fitted with constrains on Debye-Waller factors of Cu-H scatters.

Path	N[a]	σ^2 / Å^2 [b]	R_{eff} / Å [c]	R + ΔR / Å [d]	C_3 / Å^3 [e]
Cu-H	3.8(4)	0.0030 (fixed)	1.735	1.652(19)	-
Cu-P	1.4(1)	0.0024(9)	2.331	2.123(7)	-
Cu-Cu	2.0(3)	0.0093(28)	2.517	2.779(25)	0.0044(5)
Cu-Cu	1.2(2)	0.0093(28)	2.785	2.996(43)	0.0044(5)
Cu-Cu	1.0(1)	0.0039(26)	2.729	3.077(33)	0.0044(5)
Cu-P-C	8.5(1.3)	0.0047(20)	3.899	3.629(38)	0.0012(9)
Cu-C	6.8(6)	0.0047(23)	3.585	3.831(38)	0.0012(9)
Cu-C	1.3(6)	0.0049(24)	3.767	3.889(111)	0.0012(9)
Cu-Cu	1.5(2)	0.0053(20)	3.761	4.173(32)	0.0044(5)

[a] – path degeneration / coordination number (for single scattering); [b] – Debye-Waller factor; [c] – distance in structural model used for EXAFS analysis; [d] – fitted distance; [e] – third cumulant (anharmonicity).

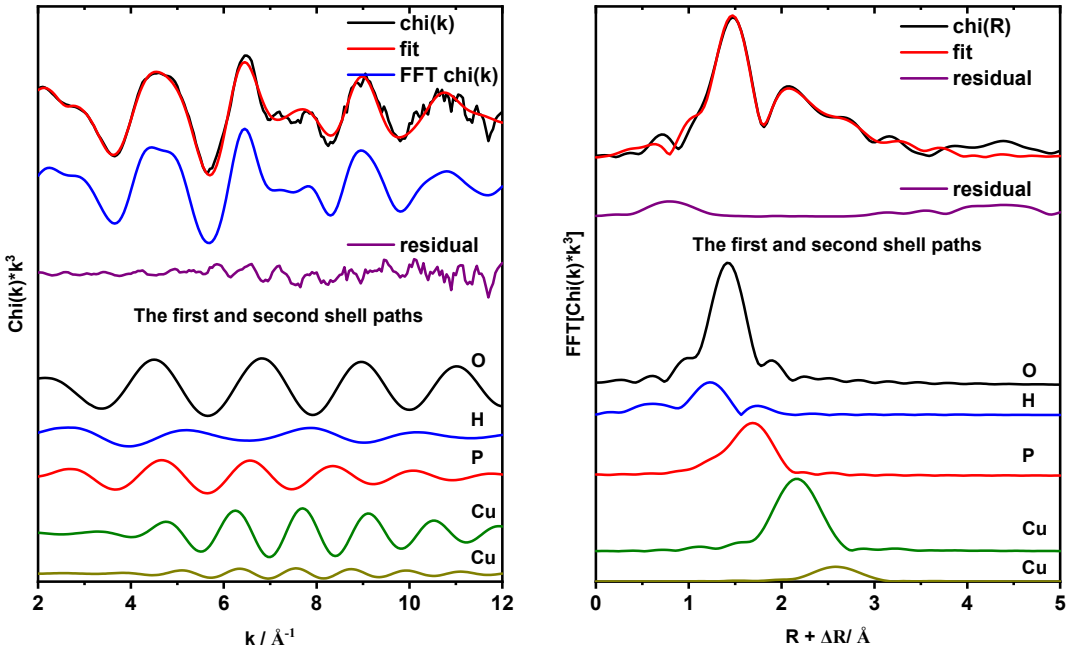

Figure S14. Left: Fourier-transformed EXAFS spectrum of **5**-ZnO compared to the fitted model, residuals and 1st and 2nd coordination shell scattering paths. Right: k-space EXAFS of **5**-ZnO compared to the fitted model, Fourier-filtered model, residual function and 1st and 2nd coordination shell scattering paths. The model was fitted with an additional Cu-O scattering path.

Table S8. Optimized EXAFS parameters for **5**-ZnO fitted with an additional Cu-O scatter.

Path	N[a]	σ^2 / Å^2 [b]	R_{eff} / Å [c]	R + ΔR / Å [d]	C_3 / Å^3 [e]
Cu-H	2.9(3)	0.0054(25)	1.735	1.568(36)	-
Cu-O	1.2(1)	0.0023(13)	1.836	1.838(12)	-
Cu-P	0.8(1)	0.0099(25)	2.331	2.155(19)	-
Cu-Cu	1.3(1)	0.0098(15)	2.517	2.514(11)	-
Cu-Cu	0.4(2)	0.0108(17)	2.785	2.957(52)	-
Cu-C	5.1(4)	0.0098(36)	3.585	3.935(29)	-
Cu-P-C	8.9(1.7)	0.0148(43)	3.899	2.962(48)	-
Cu-C	3.2(5)	0.0149(59)	3.972	3.314(33)	-

[a] – path degeneration / coordination number (for single scattering); [b] – Debye-Waller factor; [c] – distance in structural model used for EXAFS analysis; [d] – fitted distance; [e] – third cumulant (anharmonicity).

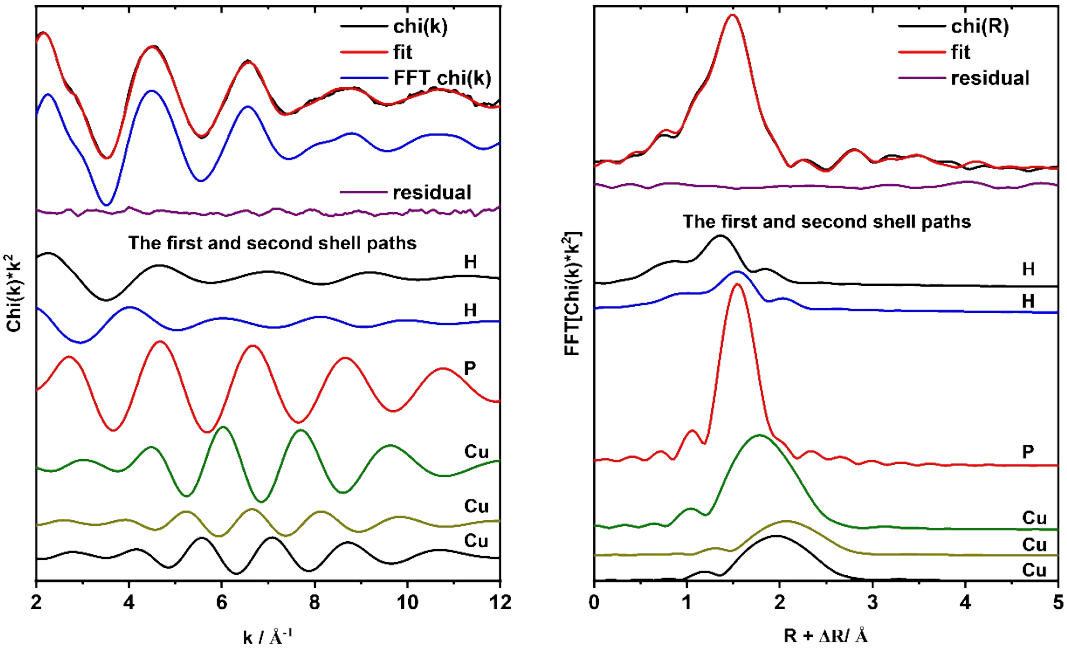

Figure S15. Left: Fourier-transformed EXAFS spectrum of **5**-ZrO_2 compared to the fitted model, residuals and 1st and 2nd coordination shell scattering paths. Right: k-space EXAFS of **5**-ZrO_2 compared to the fitted model, Fourier-filtered model, residual function and 1st and 2nd coordination shell scattering paths. The model was fitted without constraints involved.

Table S9. Optimized EXAFS parameters for **5**-ZrO_2 fitted without constraints.

Path	N[a]	σ^2 / Å^2 [b]	R_{eff} / Å [c]	R + ΔR / Å [d]	C_3 / Å^3 [e]
Cu-H	6.0(4)	0.0052(34)	1.735	1.715(21)	0
Cu-H	6.5(4)	0.0052(34)	1.995	1.908(23)	0
Cu-P	1.9(1)	0.0031(8)	2.331	2.204(8)	0.0021(1)
Cu-Cu	3.7(3)	0.0100(12)	2.517	2.752(14)	0.0055(1)
Cu-Cu	2.3(3)	0.0111(13)	2.785	2.911(21)	0.0055(1)
Cu-P-C	14.3(1.5)	0.0090(22)	3.899	3.023(19)	-0.0007(3)
Cu-Cu	1.9(2)	0.0108(13)	2.729	3.038(17)	0.0055(1)
Cu-C	4.4(4)	0.0119(27)	3.585	4.065(27)	-0.0028(2)
Cu-Cu	1.0(3)	0.0120(33)	3.761	4.043(33)	0.0022(8)

[a] – path degeneration / coordination number (for single scattering); [b] – Debye-Waller factor; [c] – distance in structural model used for EXAFS analysis; [d] – fitted distance; [e] – third cumulant (anharmonicity).

Figure S16. Left: Fourier-transformed EXAFS spectrum of **5**-ZrO_2 compared to the fitted model, residuals and 1st and 2nd coordination shell scattering paths. Right: k-space EXAFS of **5**-ZrO_2 compared to the fitted model, Fourier-filtered model, residual function and 1st and 2nd coordination shell scattering paths. The model was fitted with constraints on Debye-Waller factors of Cu-H scatters.

Table S10. Optimized EXAFS parameters for **5**-ZrO_2 fitted with constraints on Debye-Waller factors of Cu-H scatters.

Path	**N**[a]	**σ^2 / Å²** [b]	**R_{eff} / Å** [c]	**R + ΔR / Å** [d]	**C_3 / Å³** [e]
Cu-H	4.0 (fixed)	0.0020 (fixed)	1.735	1.635(56)	-
Cu-H	2.0 (fixed)	0.0031 (fixed)	1.995	1.667(115)	-
Cu-P	2.1(1)	0.0027(11)	2.331	2.212(17)	0.0020(3)
Cu-Cu	2.3(1)	0.0100(30)	2.517	2.843(43)	0.0067(9)
Cu-Cu	2.4(2)	0.0100(30)	2.785	3.014(47)	0.0067(9)
Cu-Cu	1.1(2)	0.0036(3)	2.729	3.177(43)	0.0067(9)
Cu-P-C	10.3(9)	0.0071(35)	3.899	3.743(58)	0.0087(12)
Cu-C	6.2(3)	0.0088(47)	3.585	3.826(30)	-
Cu-C	2.8(3)	0.0091(49)	3.767	3.982(81)	-
Cu-Cu	2.3(2)	0.0104(28)	3.761	4.344(53)	0.0067(9)

[a] – path degeneration / coordination number (for single scattering); [b] – Debye-Waller factor; [c] – distance in structural model used for EXAFS analysis; [d] – fitted distance; [e] – third cumulant (anharmonicity).

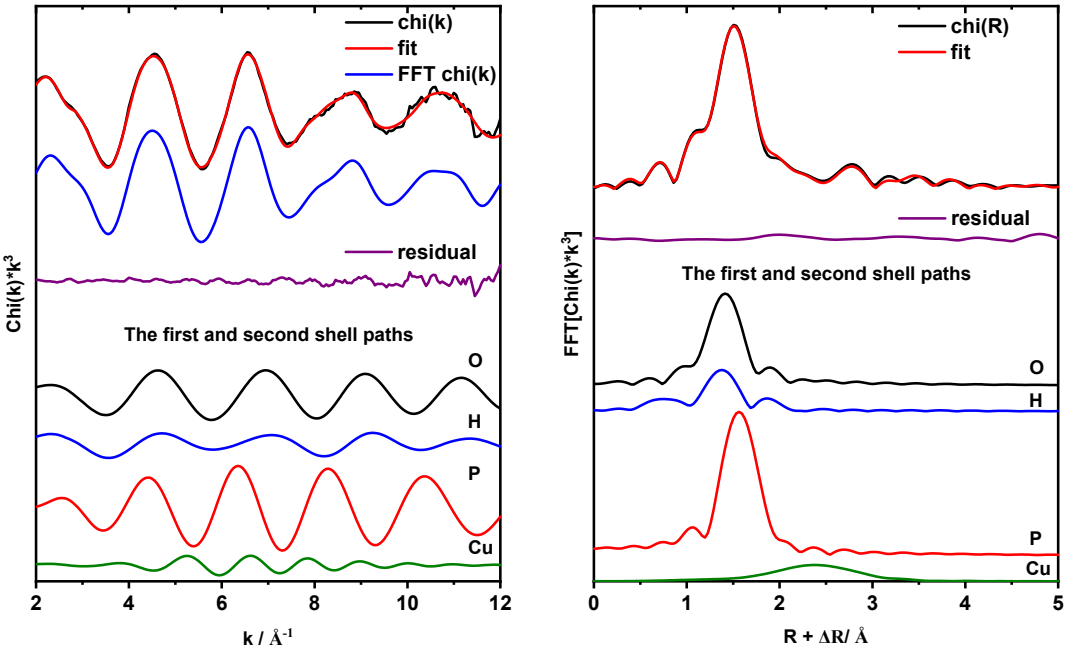

Figure S17. Left: Fourier-transformed EXAFS spectrum of **5**-ZrO_2 compared to the fitted model, residuals and 1st and 2nd coordination shell scattering paths. Right: k-space EXAFS of **5**-ZrO_2 compared to the fitted model, Fourier-filtered model, residual function and 1st and 2nd coordination shell scattering paths. The model was fitted with an additional Cu-O scattering path.

Table S11. Optimized EXAFS parameters for **5**-ZrO_2 fitted with an additional Cu-O scatter.

Path	N[a]	σ^2 / Å^2 [b]	R_{eff} / Å [c]	R + ΔR / Å [d]	C_3 / Å^3 [e]
Cu-H	3.9(1.3)	0.0031(14)	1.735	1.705(21)	0
Cu-O	1.0(1)	0.0025(15)	1.836	1.823(9)	0
Cu-P	1.3(1)	0.0035(4)	2.331	2.297(5)	0.00259(3)
Cu-Cu	1.1(1)	0.0196(15)	2.517	2.233(11)	-0.00591(22)
Cu-C	3.1(6)	0.0147(27)	3.585	3.935(29)	-0.01417(41)
Cu-P-C	6.4(5)	0.0108(17)	3.899	2.962(48)	-0.01158(44)
Cu-C	1.2(4)	0.0048(38)	3.767	3.314(33)	-0.01417(41)

[a] – path degeneration / coordination number (for single scattering); [b] – Debye-Waller factor; [c] – distance in structural model used for EXAFS analysis; [d] – fitted distance; [e] – third cumulant (anharmonicity).

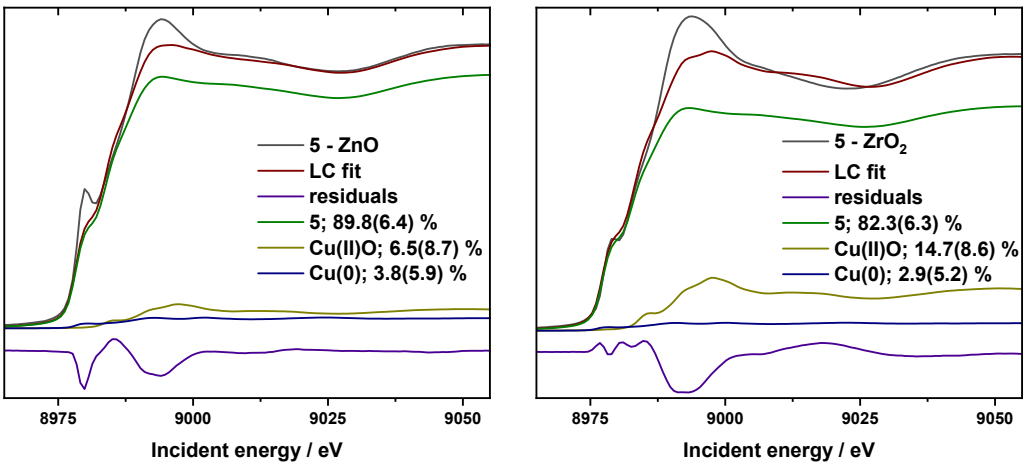

Figure S18. Left: LC fit for **5**-ZnO. Right: LC fit for **5**-ZrO_2.

Table S12. Surface OH loadings of ZrO_2 and ZnO before and after reduction with **3** and **5**.

Sample	OH conc. [mmol/g]
ZrO_2	0.32
3-ZrO_2	0.10
4-ZrO_2	0.02
5-ZrO_2	0.09
ZnO	0.19
3-ZnO	0.02
4-ZnO	0.03
5-ZnO	0.28
5-d_6-ZnO	0.29

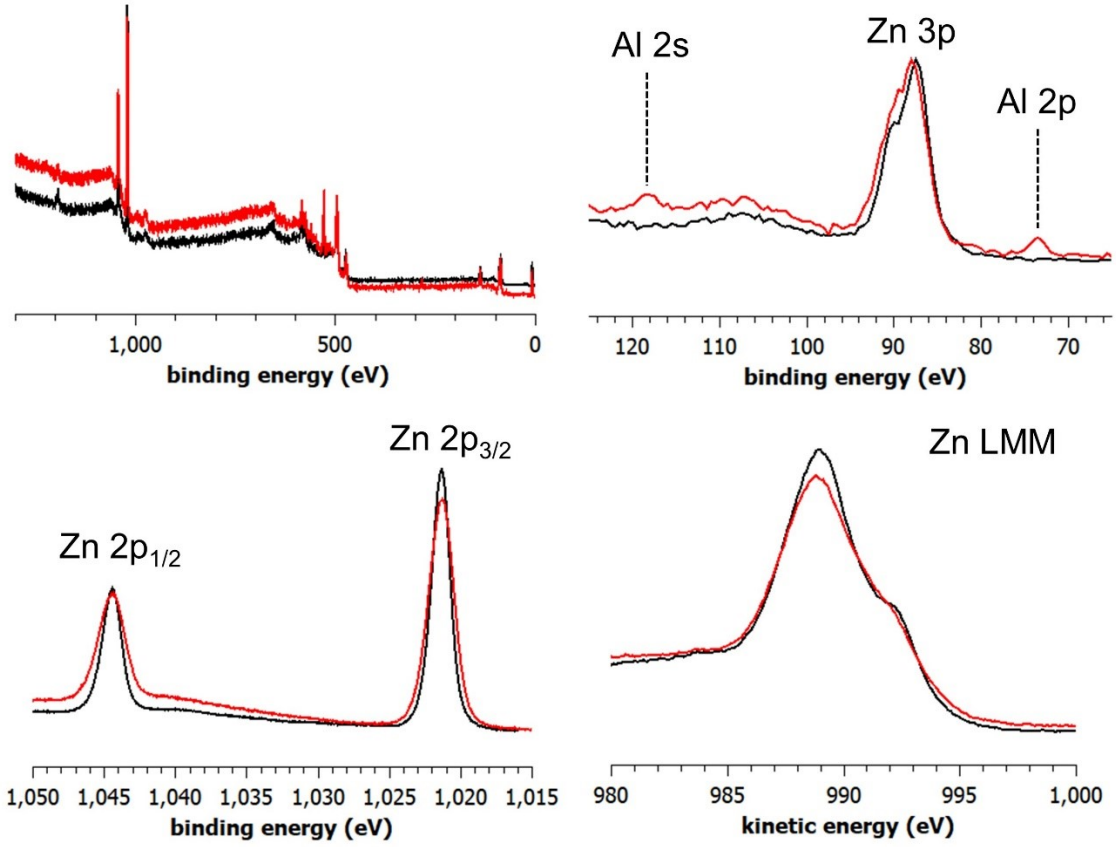

Figure S19. X-ray photoelectron spectra of both ZnO (black) and **3**-ZnO (red).

References

[1] J. Choi, M. E. Pulling, D. M. Smith, J. R. Norton, *J. Am. Chem. Soc.* **2008**, *130*, 4250.
[2] J. Choi, L. Tang, J. R. Norton, *J. Am. Chem. Soc.* **2007**, *129*, 234.
[3] S. Stoll, A. Schweiger, *J. Mag. Res.* **2006**, *178*, 42.
[4] L. Baharudin, A. C. K. Yip, V. B. Golovko, M. I. J. Polson, M. J. Watson, *Chemical Engineering Journal* **2019**, *377*, 120278.
[5] D.-w. Lee, J. Yun, *Tetrahedron Lett.* **2005**, *46*, 2037.